Electronic Supplementary Material (ESI) for Chemical Science.

Before Förster. Initial Excitation in Photosynthetic Light Harvesting.

Khadga J. Karki[1], Junsheng Chen[1], Atsunori Sakurai[2], Qi Shi[1], Alastair T. Gardiner[3], Oliver Kühn[4], Richard J. Cogdell[3] & Tönu Pullerits[1]

[1] Chemical Physics and NanoLund, Lund University, Box 124, 22100 Lund, Sweden

[2] Institute of Industrial Science, The University of Tokyo, 4-6-1 Komaba, Meguro, Tokyo 153-8505, Japan

[3] Institute of Molecular, Cell and Systems Biology, College of Medical, Veterinary and Life Sciences, University of Glasgow, Glasgow G12 8QQ, UK

[4] Institute of Physics, University of Rostock, Albert-Einstein-Str. 23-24, 18059 Rostock, Germany

1. Experimental setup

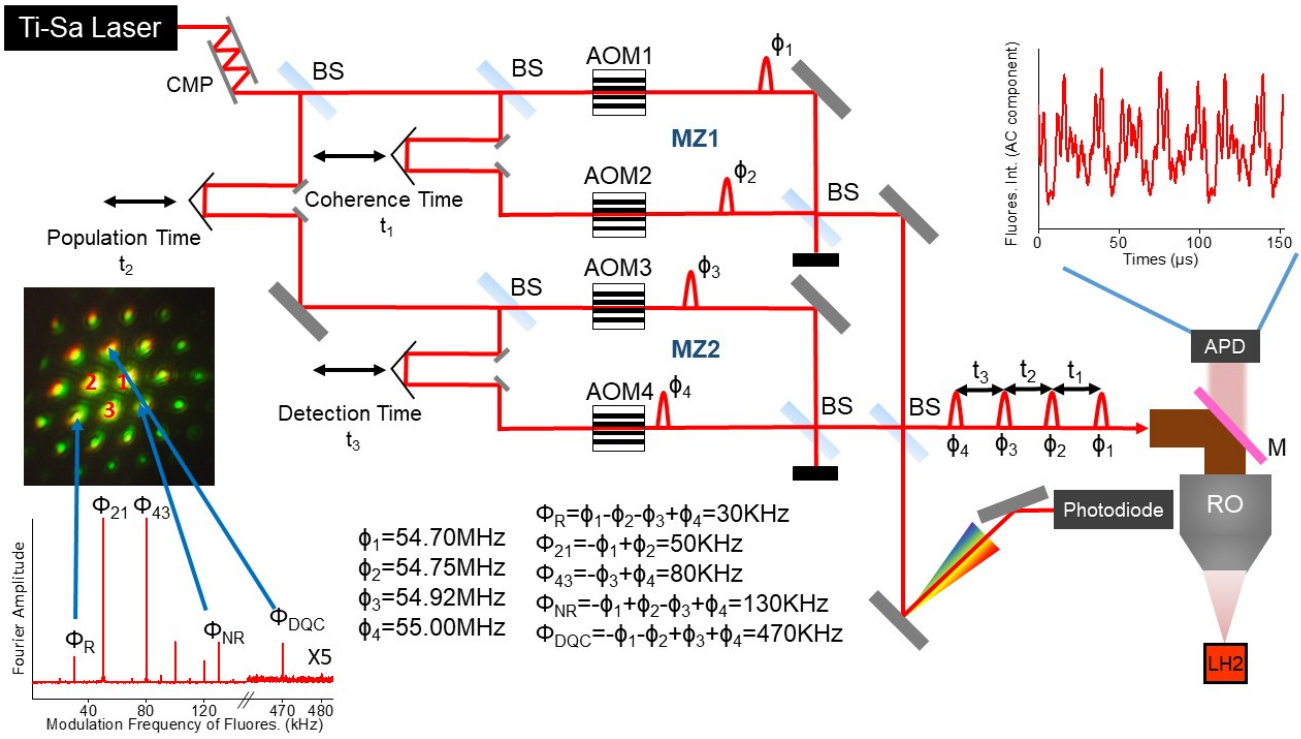

Figure S1. Schematic diagram of the FD2D setup (see text for details).

The schematic of the setup is shown in Figure S1. A Ti:Sa oscillator (Synergy, Femtolasers) provides 8-10 fs pulses at 70 MHz repetition rate. A pair of chirp mirrors (CMP) pre-compensates the group-velocity dispersion induced by the different optical elements. A beam splitter (BS) splits the pulses to two equal replicas. The pulses enter Mach-Zehnder interferometers (MZ1 and MZ2). The phases of the electric fields of the four pulses are swept using acousto-optic Bragg cells (AOM), which are placed in the arms of the MZ interferometers. The four AOMs are driven by radio frequency

generators with modulation frequencies ϕ_1=54.70 MHz, ϕ_2= 54.75 MHz, ϕ_3= 54.92 MHz and ϕ_4= 55.00 MHz, respectively. Tunable delay lines in one of the arms of each of the MZ interferometers control the coherence time t1 between pulses 1 and 2 in MZ1 and "detection time" t_3 between pulses 3 and 4 in MZ2. The pulse pairs from the MZs have a precise time delay and phase difference. An additional delay line provides timing of the pulse pairs with respect to each other giving the population time t_2 between pulses 2 and 3. All the pulses are combined collinearly with another BS. One of the outputs from the BS is directed to a grating with a groove density of 1200 l/mm. A slit is used to select a narrow frequency range of the reference at the wavelength of 815 nm. The reference is detected by an amplified photodiode. The second output of the BS is directed to an inverted microscope (Nikon Ti-S), where the sample is placed on a flow cell. A reflective objective (RO) with a numerical aperture of 0.5 focuses the beam onto the sample. The fluorescence is collected with the same objective and directed to an avalanche photodiode (APD) (LCS A3000-01, Laser Components). A dichroic mirror (FF670-SDi01-25x36, Semrock) separates the fluorescence from the excitation beam. Another long-pass filter with cutoff at 900 nm before the APD further filters out the excitation beam. The signal from the APD and the amplified photodiode (reference) are simultaneously digitized at the rate of $20x10^6$ samples per second by a 14 bit digitizer (ATS9440, AlazarTech). The data acquisition time per scanned point is 0.3 s. An example of the digitized signal is provided at the upper right corner. In the lower left the Fourier transformed signal is shown. The rephasing, the nonrephasing and the DQC signals appear at Φ_R = 30 kHz, Φ_{NR} = 130 kHz and Φ_{DCQ} = 470 kHz, respectively. The other peaks correspond to other possible pulse combinations which excite fluorescence. For example, 80 kHz is excited by pulses 3 and 4. The algorithms of generalized lock-in amplifier [1] isolate the amplitude and the phase of the signal with respect to the reference at the frequencies Φ_R, Φ_{NR} and Φ_{DCQ}. Note that the reference has signals only at the frequencies ϕ_x- ϕ_y, where x and y index the four modulation frequencies of the AOMs. These signals are digitally mixed to obtain the phase of the reference at Φ_R, Φ_{NR} and Φ_{DCQ}. Also shown is the image of the phase-matched signals in conventional 3-pulse photon echo spectroscopy. 1, 2 and 3 are the three laser beams which have passed the sample. All other spots are phase-matched photon echo signals. The correspondence between the three signals used in the current work is indicated by arrows.

The real and the imaginary part of the rephasing and the non-rephasing 2D spectra are obtained by scanning the time delay between the pulses of each pair (pulses 2-1 and pulses 4-3). Time delay between pulse 3 and 2 is fixed at 0 fs. A time step of 6 fs along both the time delay axes is used in the scans. The range of scan along both the axes is 240 fs. Phasing of the time domain data is done by setting the phase at initial time delays to be zero (i.e. at t_{21}=t_{43}=0 fs, the signal has no imaginary component). The time domain data is Fourier transformed to obtain the 2D spectra in frequency domain. The Fourier transform along the time delay between the pulses 2 and 1 provides the frequency of the pump pulse sequence (usually denoted as ω_1 or ω_{21}). Similarly, the Fourier transform along the time delay between the pulses 4 and 3 provides the frequency of the probe pulse sequence (usually denoted as ω_3 or ω_{43}) [2,3].

2. <u>LH2 sample preparation.</u>

LH2 complexes from *Rhodopseudomonas acidophila* 10050 were isolated by method described elsewhere [4]. The isolated LH2 complexes were dispersed in 25 mM Tris-HCl buffer (PH=8.0) containing 0.1% N,N-Dimethyldodecylamine N-oxide (LDAO). The optical density (at 850 nm) of the solution in a 1 cm pathlength quartz cuvette (flow cell) was 0.3. The LH2 solution was deoxygenated by adding an oxygen scavenging system: catalase (0.35 µM), glucose oxidase (3 µM) and glucose (0.1 M) [5]. The sample was circulated through the cuvette using a peristaltic pump providing flow speed 5 l/min during the data acquisition.

3. Sign of the signal in nonlinear spectroscopy

For better understanding and more transparent interpretation the nonlinear spectroscopy signals are usually discussed in terms of ground state bleach (GSB), stimulated emission (SE), excited state absorption (ESA) and the double quantum coherence (DQC) contributions [6]. In transient absorption spectroscopy usually an intuitive convention is followed that GSB and SE are considered negative (absorption of the probe beam is reduced due to the pump) and ESA is positive (more absorption because of the pump) [7]. Usually DQC is ignored in transient absorption since it only plays a role for negative pump-probe delays and during pulse overlap. In coherent heterodyne detected 2D spectroscopy (HD2D) the sign convention is opposite to the transient absorption – GSB and SE are shown as positive and ESA as negative. The HD2D sign convention follows the Feynman diagram rules [8] giving the sign of the signal as $(-1)^n$, where n is the number of interactions from the right in the diagram. This rule originates from the perturbative expansion of the density matrix in powers of the electric field of the laser – each time the interaction with the field acts from the right in a commutator, it comes with the minus sign. The rule is very useful for relating the different signal components to each other – it is not always intuitively obvious which parts of the signal should have opposite signs and cancel [9]. As long as the relation between the signs of the different signal components is consistent, the total sign is a matter of conventions as we could see from the comparison of the transient absorption and HD2D. Since HD2D and FD2D signals are closely related, it would be convenient to have the same sign convention for these two methods – the GSB and SE signals would be positive.

In fact, there is even a more formal reasoning for the above convention. We start with the description of the HD2D and FD2D signals. The first is related to the third order polarization

$$P^{(3)} \equiv tr\{\hat{\mu}(t)\hat{\rho}^{(3)}(t)\}, \qquad \text{(S1)}$$

while the FD2D is due to the fourth order excited state population

$$\hat{A}^{(4)}(t) \equiv tr\{\hat{A}(t)\hat{\rho}^{(4)}(t)\}, \text{(S2)}$$

where $\hat{A} = \sum_{\nu} |\nu\rangle\langle\nu|$ is a projector to all excited states which can give fluorescence. In HD2D the third order density matrix contains three nested commutators providing interactions with the electric field via the transition dipole moment while the fourth transition dipole moment appears when the polarization $P^{(3)}$ which generates the signal, is calculated. The signal generating interaction is taken from the left by the convention. In FD2D the fourth order density matrix contains an additional commutator and all four interactions are with the incoming fields. Thereby the usual Feynman diagram rules would mean negative GSB and SE signals (see Fig S2). However, the general expression of the k-th order density matrix has a prefactor $(-1)^k$ which would give us an additional minus in FD2D leading to the same GSB and SE signs as in HD2D. Such sign convention has been used in previous FD2D literature [2,10] and we are following this in our work making comparison with HD2D literature more clear. It should be pointed out that in the experiment, the sign of the signal is not known.

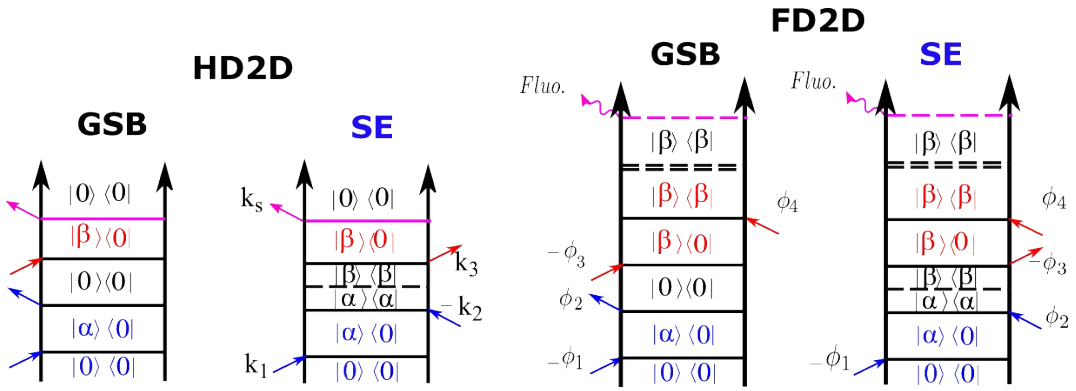

Figure S2. Nonrephasing Feynman diagrams for the ground state bleach (GSB) and stimulated emission (SE) of the αβ cross peak. Left HD2D and right FD2D. The Feynman diagram sign rule would say that in HD2D the GSB and SE are positive but in FD2D negative. Usual convention, however, is to have GSB and SE in both experiments positive.

4. <u>ESA signal cancellation.</u>

We call the electronic states responsible for the B800 and B850 bands as |α> and |β>, respectively. The molecular (site) excitations of the two LH2 rings are |a> and |b>, the latter being the densely packed ring, see figure 2. We can write

$$|\alpha\rangle = \sum_{a,b}\left(c_{\alpha a}|a\rangle + c_{\alpha b}|b\rangle\right)$$
$$|\beta\rangle = \sum_{a,b}\left(c_{\beta a}|a\rangle + c_{\beta b}|b\rangle\right) \quad , \qquad \text{(S3)}$$

where the coefficients $c$are the exciton amplitudes at the different sites. Usually $c_{\alpha b}$ and $c_{\beta a}$ are considered negligible and the B800 and B850 bands are related to the BChl molecules |a> and |b>, respectively [11]. Analogously, the states |σ> of the doubly excited manifold responsible for the broad excited state absorption are expressed as

$$|\sigma\rangle = \sum_{a,b} cc_{\sigma ab}|a\rangle|b\rangle + \sum_{a\neq a'} cc_{\sigma aa'}|a\rangle|a'\rangle + \sum_{b\neq b'} cc_{\sigma bb'}|b\rangle|b'\rangle +$$
$$+ \sum_{a^*} cc_{\sigma a^*}|a^*\rangle + \sum_{b^*} cc_{\sigma b^*}|b^*\rangle \quad , \qquad \text{(S4)}$$

where the coefficients $cc$are the double exciton amplitudes and the high energy molecular states $|a^*\rangle$ can be reached from the lowest energy excited state $|a\rangle$ by absorption of light from the laser pulse [12]. The assignment of the molecules, the energy levels, the corresponding linear absorptions and the generic 2D absorption are shown in Fig 2 of the main article.

All possible ESA pathways can be paired up as shown in Figure S3 where $|\varphi\rangle$ and $|\varphi'\rangle$ can be any state $|\alpha\rangle$ or $|\beta\rangle$. The doubly excited manifold rapidly relaxes to the singly excited manifold via exciton annihilation [13]. Since exactly the same transitions are always involved in both two pathways, the corresponding signal strengths are the same. However, according to the Feynman diagram sign rules, these signals have opposite signs and cancel each other. Consequently, systems with rapid exciton annihilation as individual light harvesting complexes or, in general, excitonic systems, do not show an ESA signal in the FD2D experiment. Such rapid annihilation limit which takes place in

individual antenna complexes like detergent isolated LH2 complexes here should not be confused with the diffusion-driven incoherent exciton-exciton annihilation which usually occurs on a much longer time scale [14] (see also section S6).

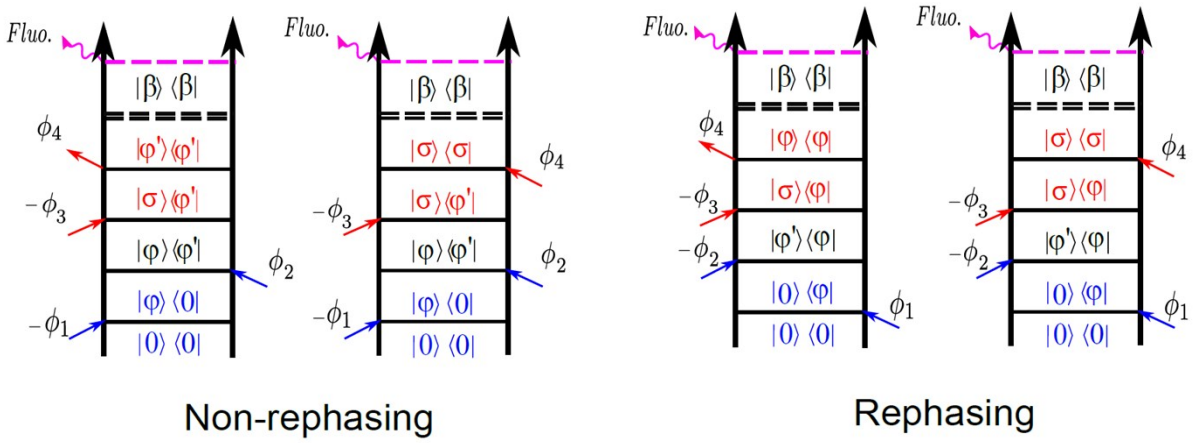

Figure S3. General non-rephasing and rephasing Feynman diagrams providing all possible Liouville pathways of ESA. The diagrams of all such pairs have the same amplitudes since the doubly excited state rapidly relaxes to the singly excited level without giving any significant emission. At the same time the diagrams have opposite signs, thereby they cancel each other.

5. Lower cross peak in HD2D and two-color pump-probe spectroscopy

Earlier two-color pump-probe (pump at B800, probe at B850) [15] and the HD2D measurements [16,17] have shown only negligible signal at the B800 excitation – B850 detection region at zero population times. In pump probe experiment the population time is simply the time delay between the pulses. In those experiments the bleach/stimulated emission signal grows with population time which has been taken as evidence for B800 to B850 energy transfer. The corresponding time constant of the exponential rise, 700 fs, is the B800 to B850 transfer rate [18] . The apparent controversy between the FD2D results here and those earlier experiments can be resolved by realizing that the ESA signal, present in those earlier measurements, leads to cancellation of the total signal at earlier times. In Figure S4 we show the different signal components (GSB, SE and ESA) in case of FD2D and HD2D (the same as pump-probe) for the lower cross peak. The bleach signal at zero time is present in both experiments but is canceled out by the ESA in case of HD2D. The Feynman diagrams giving the different signal components are also provided. For each GSB pathway there is always an ESA1 pathway which cancels it unless there is an ESA2 pathway which cancels the ESA1 as in FD2D.

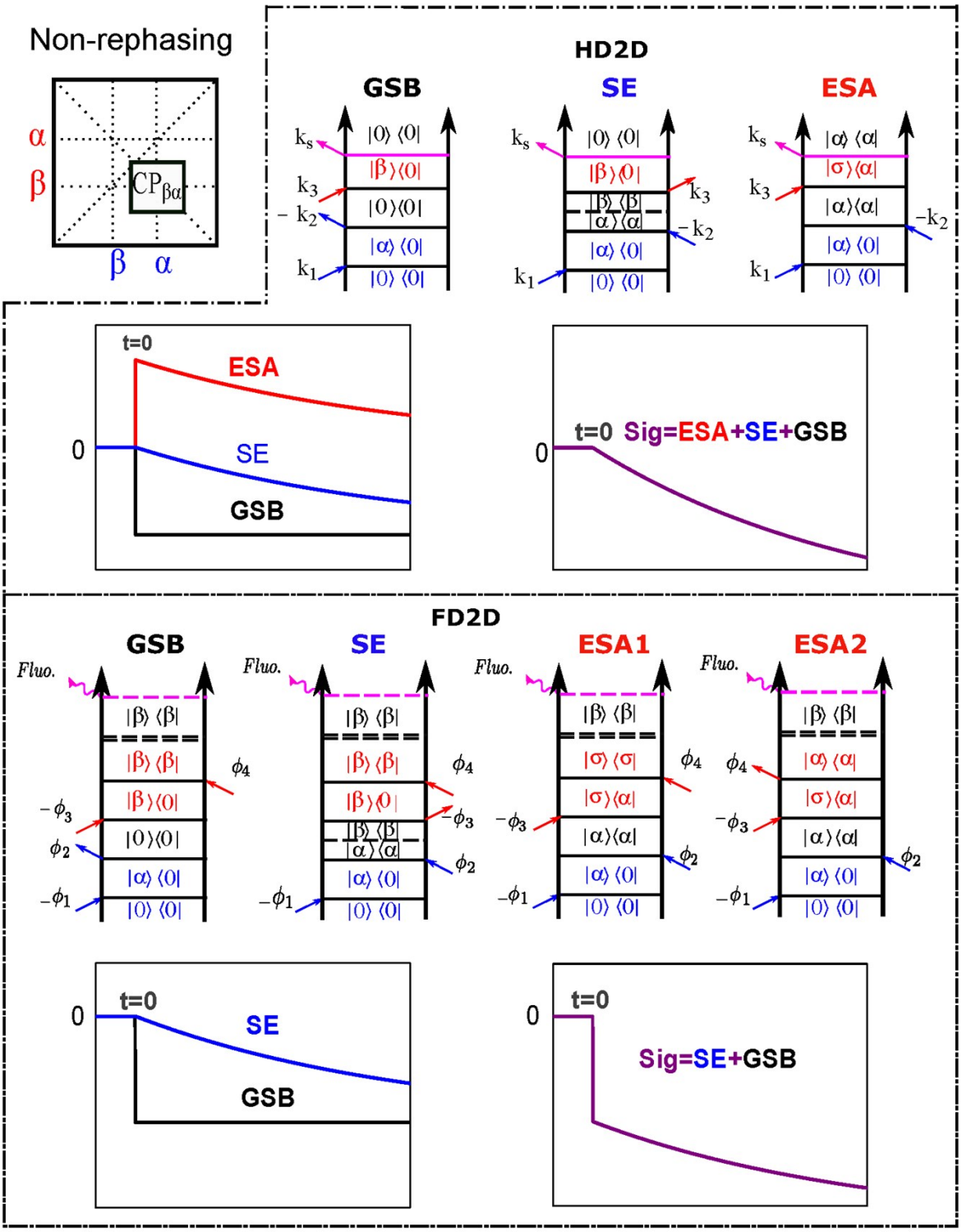

Figure S4. Nonrephasing contributions for the lower cross peak. Upper panel shows the Feynman diagrams of GSB, SE and ESA signals of the HD2D and pump probe experiments. In the pump-probe

experiment $\mathbf{k}_1$ and $-\mathbf{k}_2$ come from the same pulse. To be at the cross peak, the doubly excited state $|\sigma\rangle = |\alpha\beta\rangle$. At time zero the GSB and ESA signals cancel each other and since there is no SE signal possible yet because of $|\alpha\rangle$ to $|\beta\rangle$ relaxation has not had time to occur, the signal vanishes. Below the time evolution of the different signal components and their sum is shown. Lower panel shows the same for FD2D. Now there are two ESA pathways which cancel each other. Consequently, there is strong GSB signal present at t=0.

6. Upper exciton band edge of B850 and the cross peaks

Numerous studies have identified absorption of LH2 at around 780 nm as weakly absorbing upper excitonic band edge of B850[19]. Such upper excitonic band could lead to the cross peaks. However, we see 800-850 cross peaks, not 780-850 cross peaks. Second, the transition dipole moment of the upper excitonic component is very weak and thereby cannot explain the pronounced cross peaks we observe. Furthermore, such cross peaks would have even appeared in HD2D but they do not. We conclude that the upper excitonic component of the B850 cannot explain the observed cross peaks.

7. 2D of a weakly coupled heterodimer

In case of a coupled heterodimer ab, see Figure S5 left, the shifts of the energy levels and corresponding mixing of the states α and β is not large for the case where the coupling is smaller than the energy difference. The transitions corresponding to the energy eigenstates (excitons) α and β are quite similar to the transitions of the monomeric units a and b. Inspection of the ESA Feynman pathways leads to conclusion that significant cancellation of the GSB by the ESA should occur but since still considerable mixing of the a and b states together with the energy level shifts occur, the cancellation is not perfect. In case of weaker coupling – right side, the ESA cancels the bleach almost perfectly.

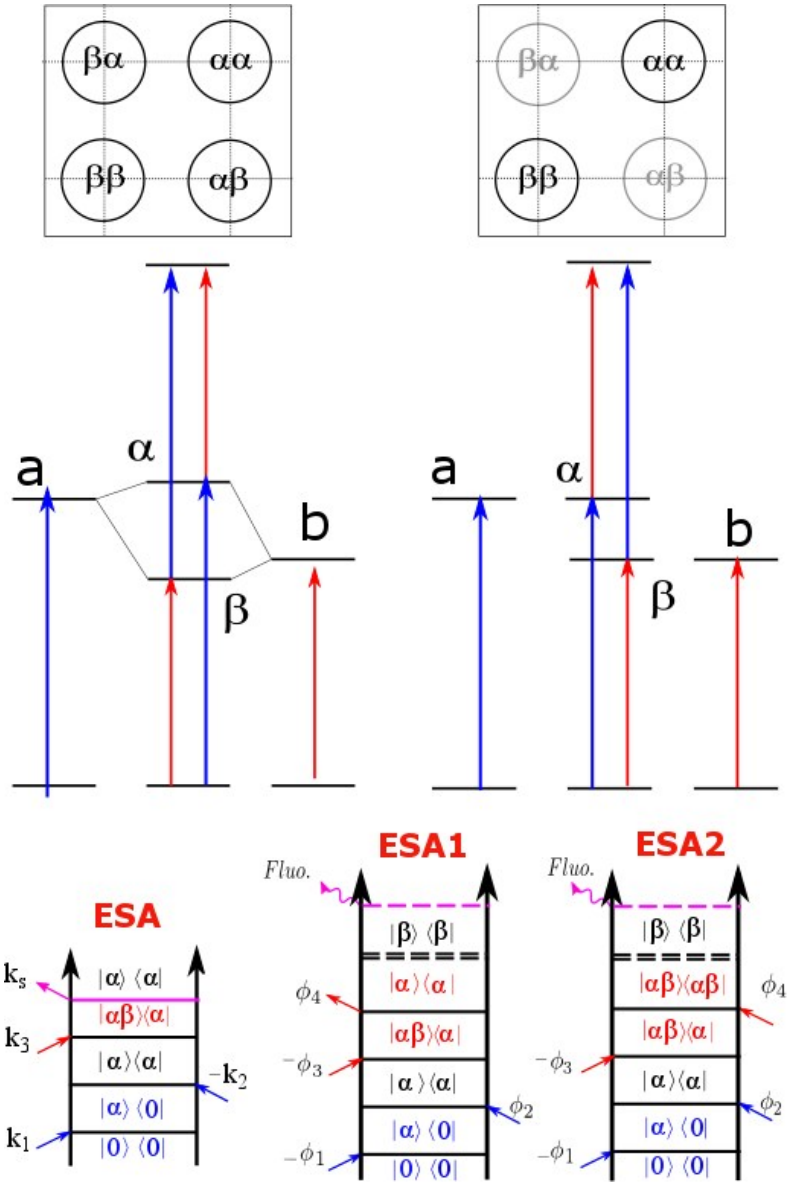

Figure S5 Weakly coupled heterodimer model. At the left side the coupling is strong enough to cause the shift of the energy levels and mixing of the transitions. Consequently, the cancellation of the ESA and GSB is not perfect. If the coupling is very weak, α and β are almost the same as a and b monomeric transition and the GSB is cancelled by ESA. The doubly excited state σ is explicitly written out as |αβ> for clarity.

8. <u>What happens when the coupling J is approaching 0?</u>

In the limit of approaching zero interaction the annihilation cannot take place anymore and the pathway where both states are excited (doubly excited state) would give two units of signal, instead of one in case of annihilation and the ESA signal would not cancel. This limit rises a number of interesting follow up questions. For example, what disappears before, the correlated bleach or annihilation? Such questions cannot be answered theoretically but need careful experimental investigation. In this limit also the correlated emission from two independent excited systems needs to be considered. As we argue in the following section, our measured signals behave differently from what is predicted for the correlated two-body fluorescence.

9. DQC signal

In DQC pathways the first two pulses make a coherence between the doubly excited levels and the ground state. All possible DQC pathways are presented in Figure S6. The diagrams that cancel out each other are paired up. After cancellation, only six diagrams remain, four of which will be at the diagonal. For the cross peaks we have one diagram per each feature of the 2D spectrum. The doubly excited states involved in the double quantum coherences of the pathways for the non-diagonal signals involve both B800 and B850. Such double quantum coherence state can lead to a signal only if B800 and B850 are correlated.

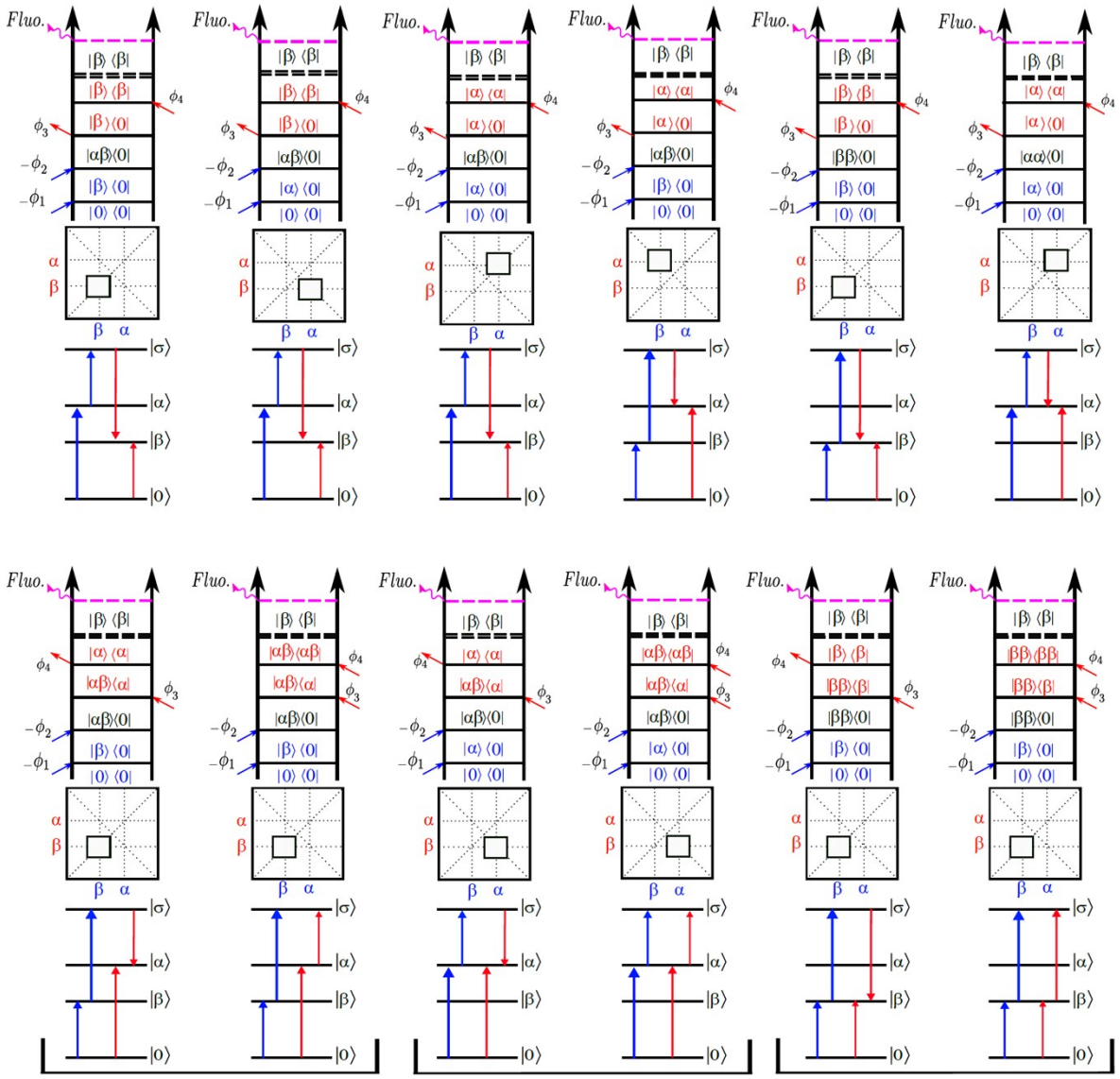

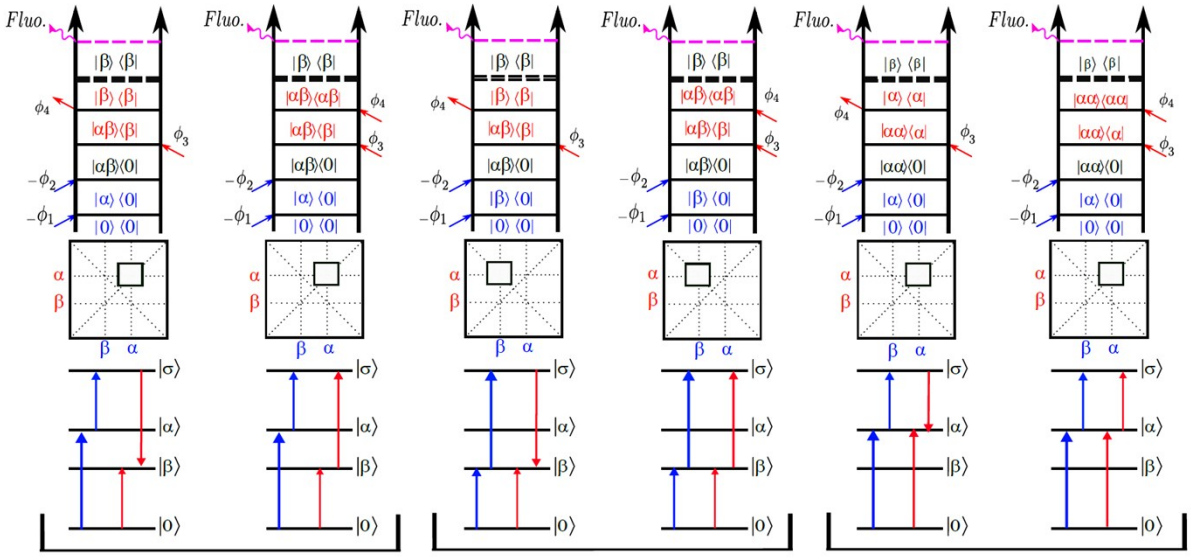

Figure S6. All possible DCQ Feynman diagrams. The two lower rows add up to zero. The diagrams which cancel each other are paired up. Only the upper row remains. The upper and lower cross peaks originate from a single diagram each which is in the double quantum coherence $|\alpha\beta\rangle\langle 0|$ after two pulses.

Recent theoretical analysis has shown that the signals at higher modulation frequencies relevant for multi-quantum coherence can arise due to a simple correlation of the excitations [8]. Presence of such correlations leads to multi-quantum coherence signals at long time delays. It is important to carry out experiments at excitation intensities where such effects are negligible. The effects can also be checked during the experiments by monitoring the relevant signals at longer time delays. As shown in Figure S7, the Fourier transform of the signals at time delays t_{21}= 50 fs, t_{32}= 0 fs and t_{43}=50 fs does not show any signal at 470 kHz (DQC signal modulation frequency), while there are still very pronounced two-pulse signals present (for example 50, 80 and 250 kHz). This ascertains that the effects of the statistical correlation is negligible in the experimental conditions we have used.

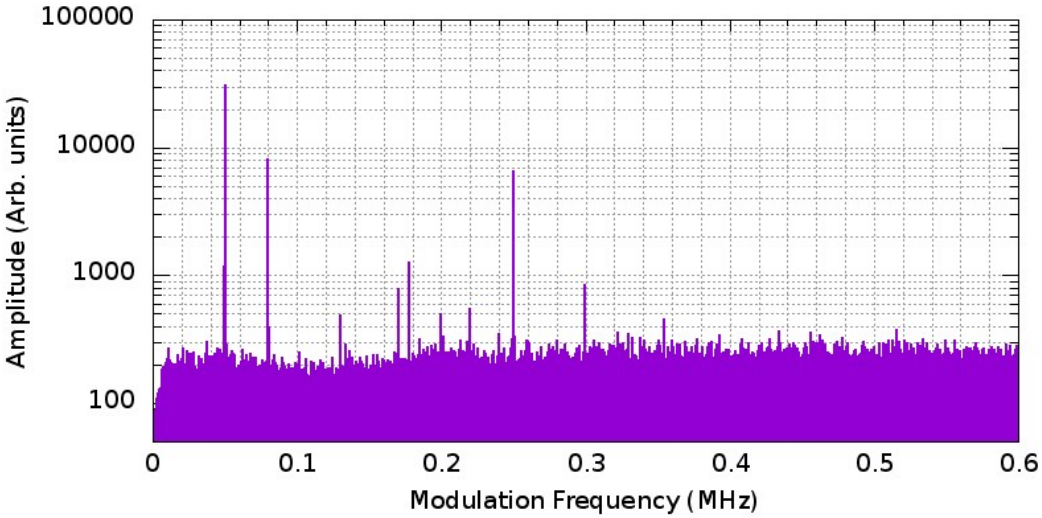

Figure S7. Fourier transform of the raw data acquired at t21=t43= 50 fs. No signal can be observed at the modulation frequency of 470 kHz corresponding to the signal due to the DQC.

Alternatively, one can also measure the dephasing of the signals at $\phi_{21} = \phi_2 - \phi_1$ and $2\phi_{21}$ to check for the artifacts due to statistical correlations. Figure S8 shows the real and imaginary parts of the signals at 50 kHz and 100 kHz. The signal at 50 kHz is the linear response, while the signal at 100 kHz is the DQC signal from the excitation involving only the first two pulses. It can be clearly seen, that if the time step of the linear signal would be twice shorter, it would not resemble the DQC signal as would be the case for a simple statistical correlation.

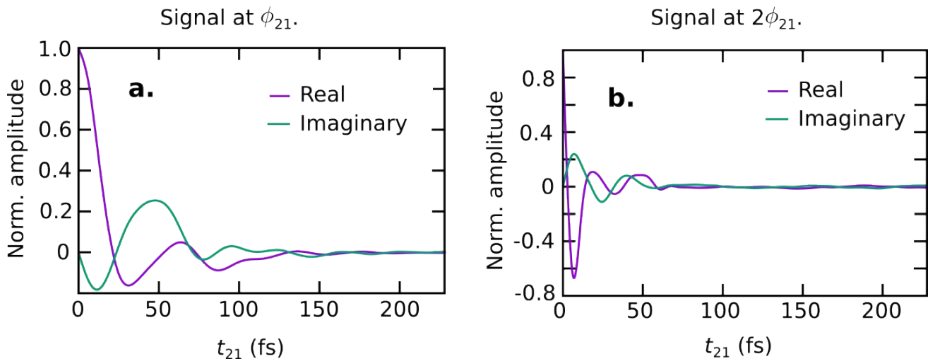

Figure S8. Real and imaginary part of the signals at 50 kHz (a) and 100 kHz((b). The signal at 100 kHz dephases much more rapidly than the signal at 50 kHz.

References.

1 S. Fu, A. Sakurai, L. Liu, F. Edman, T. Pullerits, V. Öwall and K. J. Karki, *Rev. Sci. Instrum*., 2013, **84**, 115101.

2 P. F. Tekavec, G. A. Lott and A. H. Marcus, *J. Chem. Phys.*, 2007, **127**, 214307.

3 F. A. Damtie, A. Wacker, T. Pullerits and K. J. Karki, *Phys. Rev. A.*, 2017, **96**, 053830.

4 M. Z. Papiz, A. M. Hawthornthwaite, R. J. Cogdell, K. J. Woolley, P. A. Wightman, L. A. Ferguson and J. G. Lindsay, *J. Mol. Biol.*, 1989, **209**, 833–835.

5 S. Tubasum, R. J. Cogdell, I. G. Scheblykin and T. Pullerits, *J. Phys. Chem. B.*, 2011, **115**, 4963–4970.

6 N. Christensson, F. Milota, A. Nemeth, I. Pugliesi, E. Riedle, J. Sperling, T. Pullerits, H. F. Kauffmann and J. Hauer, *J. Phys. Chem. Lett.*, 2010, **1**, 3366–3370.

7 G. Trinkunas, J. L. Herek, T. Polívka, V. Sundström and T. Pullerits, *Phys. Rev. Lett*., 2001, **86**, 4167–4170.

8 S. Mukamel, *J. Chem. Phys.*, 2016, **145**, 041102.

9 N. Christensson, F. Milota, A. Nemeth, J. Sperling, H. F. Kauffmann, T. Pullerits, J. Rgen Hauer and J. Hauer, *J. Phys. Chem. B.*, 2009, **113**, 16409–19.

10 G. A. Lott, A. Perdomo-Ortiz, J. K. Utterback, J. R. Widom, A. Aspuru-Guzik and A. H. Marcus, *Proc. Natl. Acad. Sci.*, 2011, **108**, 16521–16526.

11 T. Pullerits and V. Sundström, *Acc. Chem. Res.*, 1996, **29**, 381–389.

12 P. Kjellberg, B. Brüggemann and T. Pullerits, *Phys. Rev. B - Condens. Matter Mater. Phys.*, 2006, **74**, 024303.

13 B. Brüggemann, J. L. Herek, V. Sundström, T. Pullerits and V. May, *J. Phys. Chem. B.*, 2001, **105**, 11391–11394.

14 F. W. & T. B. Jakub Dostál, Franziska Fennel, Federico Koch, Stefanie Herbst, *Nat. Commun.*, 2018, **9**, 2466.

15 J. L. Herek, N. J. Fraser, T. Pullerits, P. Martinsson, T. Polívka, H. Scheer, R. J. Cogdell and V. Sundström, *Biophys. J.*, 2000, **78**, 2590–2596.

16 E. Harel and G. S. Engel, *Proc. Natl. Acad. Sci.*, 2012, **109**, 706–711.

17 M. Ferretti, R. Hendrikx, E. Romero, J. Southall, R. J. Cogdell, V. I. Novoderezhkin, G. D. Scholes and R. Van Grondelle, *Sci. Rep*., 2016, **6**, 20834.

18 S. Hess, F. Feldchtein, A. Babin, I. Nurgaleev, T. Pullerits, A. Sergeev and V. Sundström, *Chem. Phys. Lett.*, 1993, **216**, 247–257.

19 M. Pajusalu, M. Rätsep, G. Trinkunas and A. Freiberg, *ChemPhysChem.*, 2011, **12**, 634–644.